Simulation of radiation damping in rings, using stepwise ray-tracing methods

F. Méot
Brookhaven National Laboratory,
Upton, NY, 11973, USA
E-mail: fmeot@bnl.gov

April 24, 2015

Abstract

The ray-tracing code Zgoubi computes particle trajectories in arbitrary magnetic and/or electric field maps or analytical field models. It includes a built-in fitting procedure, spin tracking, many Monte Carlo processes. The accuracy of the integration method makes it an efficient tool for multi-turn tracking in periodic machines. Energy loss by synchrotron radiation, based on Monte Carlo techniques, had been introduced in Zgoubi in the early 2000s for studies regarding the linear collider beam delivery system. However, only recently has this Monte Carlo tool been used for systematic beam dynamics and spin diffusion studies in rings, including the eRHIC electron-ion collider project at the Brookhaven National Laboratory. Some beam dynamics aspects of this recent use of Zgoubi capabilities, including considerations of accuracy as well as further benchmarking in the presence of synchrotron radiation in rings, are reported here.

Keywords: Accelerator modelling and simulations; Beam dynamics; Beam Optics; Synchrotron radiation

Contents

1 Introduction

Stochastic SR was first introduced in the Zgoubi code [1, 2, 3] in 2000 [4], for assessing emittance perturbation in the beam delivery system of the "Tesla Test Facility" (an early, European, test version of the "Linear Collider"). The Monte Carlo source code introduced in Zgoubi was drawn from the DYNAC particle dynamics code developed at Saclay in the late 1980s, by the author and others [5] - SR simulations in DYNAC were used in the design of the recirculating arcs in the "ALS" and "ELFE" electron recirculator projects [6, 7]. The present report provides detailed numerical analysis of the damping effects on beam dynamics in rings, and shows the accuracy of the data so obtained, by thorough comparison with theoretical expectations. For part of it, this work is concerned with benchmarking, which is motivated by on-going activities regarding high energy machine projects as the electron-ion collider eRHIC [8] at BNL (RHIC is the relativistic heavy ion collider), which also require spin tracking, a capability of Zgoubi [9] which had motivated its use in recent design studies regarding the e^+-e^- asymmetric collider project super-B [10].

It is planned, in a near future, to further report on similar thorough dynamics simulations regarding the effects of SR on polarization, in electron recirculators and in rings, as spin diffusion - such spin dynamics studies are being carried out at present and yield expected results, in concert with the use of the code in the design of a "fixed field alternating gradient" version of the eRHIC electron recirculator of the Electron-Ion Collider project at BNL [11].

Note that SR loss simulation can be found in other codes, possibly based on different methods. For instance, element slicing, imparting energy kicks after each slice, using either Gaussian statistics or Monte Carlo photon emission, as in elegant [12], or SAD [13], spline interpolation to the standard radiation integrals, as in BMAD [14]. The MAD code [15] as well has provision for particle tracking with quantum effects of synchrotron radiation. Other methods include applying an average energy loss at a reduced number of steps, and on that average applying an algebraic (positive or negative) random energy correction to restore the stochasticity. Advantages or drawbacks may be found in one or the other of these methods, depending on the objectives, as CPU time, accuracy. Many of these codes are documented, their SR functionalities have been subject to publications, possibly including benchmarking exercises, comparisons between codes can be found [16].

Finally, amongst other interests seen in developing SR in Zgoubi, the code allows tracking in field maps (of light source-style "insertion devices" for instance [17, 18]) in addition to the numerous analytical models of magnetic fields that it provides. The stepwise method allows one to take advantage of modern 3-D magnet design codes (including space and time evolution of fields), based on a number of built-in means for a direct use of the field maps which these codes produce. In a different register, possible disadvantage in the matter of CPU time in the case of numerical stepwise integration (compared to much faster kick-drift techniques for instance) is (i) possibly balanced by the accuracy in field modeling, and (ii) mitigated by the possibility of using multi-core clusters, a very common strategy in polarization studies [11, 19, 20, 21] performed on CPU farms as NERSC [22]. More on these aspects can be found in [1].

2 The ray-tracing code Zgoubi

2.1 Introduction

The ray-tracing code Zgoubi [1, 2] computes trajectories of charged particles in arbitrary number, in optical assemblies built from analytical models of fields and/or in magnetic or electric field maps. The code contains a built-in fit procedure, spin tracking, in-flight decay and several other Monte Carlo process simulations[1]. It also provides synchrotron radiation (SR) calculation, on the one hand the spectral-angular radiation from particle motion, used for instance to understand and fix issues of negative interferences at LEP [24], and for the design of the SR based beam profile monitoring installations at LHC [25], on the other hand the energy loss and dynamical effects on particle motion, the subject of this report. SR capabilities include the handling of undulator radiation [17, 25, 18]. Development of coherent SR modelling has been undertaken in the early 2000s, in view of bunch compression chicane design studies, yet not released so far. The high accuracy of the numerical method in Zgoubi[2] is well illustrated in a number of tracking simulations requiring up to millions of turns, for instance polarized proton acceleration ramp through strong depolarizing snake resonances at the RHIC collider [20], or full acceleration cycle simulations in RHIC injector, the alternating gradient synchrotron (AGS) [21].

2.2 Synchrotron radiation in Zgoubi

The details of the numerical method for the step by step integration of particle and spin motion can be found in Zgoubi Users' Guide [2], the following focuses on the simulation technique regarding the effects of synchrotron radiation on the dynamics.

SR effects are introduced by modifying the particle vector momentum following an integration step. The next sections describe the main aspects of the technique, a general theoretical treatment can be found in Ref. [26, 27].

2.2.1 Energy loss

Given a particle travelling in the magnetic field of an arbitrary optical element or field map, Zgoubi will compute the energy loss due to stochastic photon emission, and update the particle momentum as a result of that effect, at each integration step. The energy loss is calculated in a classical manner, based on two random processes, namely,

- probability of emission of one or more photons, by a particle with rigidity $B\rho$ (energy E), over an integration step Δs, under the effect of $1/\rho$ curvature,

$$p(k) = \frac{\Lambda^k}{k!} e^{-\Lambda} \qquad \text{with} \quad \Lambda =< k >=< k^2 > \tag{1}$$

with $\Lambda = \frac{5er_0}{2\hbar\sqrt{3}} B\rho \frac{\Delta s}{\rho}$ the average number of photons radiated over Δs ($r_0 = e^2/\,4\pi\epsilon_0 m_0 c^2$ is the classical radius of the electron, e the elementary charge, m_0 the electron rest mass, $\epsilon_0 = 1\,/\,36\pi 10^9$, $\hbar$ is the Plank constant),

- energy ϵ of the emitted photon(s), following the probability

$$\mathcal{P}(\epsilon/\epsilon_c) = \frac{3}{5\pi} \int_0^{\epsilon/\epsilon_c} \frac{d\epsilon}{\epsilon_c} \int_{\epsilon/\epsilon_c}^{\infty} K_{5/3}(x) dx \tag{2}$$

[1] Collective effects may be taken into account in terms of point transforms, space charge for instance has been developed in Zgoubi [23], whereas present eRHIC studies [8] motivate the introduction - on-going - of wake fields for their contribution to momentum spread.

[2] Note that numerical integration in Zgoubi, while accurate, with the accuracy controlled via the order of the integrator or via the integration step size [1, 2], is not symplectic *strictu sensu*, since it is based on *truncated* Taylor series of position and velocity vectors.

with $K_{5/3}$ the modified Bessel function, $\epsilon_c = 3\hbar\gamma^3 c/2\rho$ the critical energy of the radiation ($\gamma = E/E_0$ with $E_0 = m_0c^2$ the rest energy).

2.2.2 Dynamical effects

The correction to the particle energy is obtained by summation of the individual energies (Eq. 2) of the k photons (Eq. 1) emitted along Δs.

SR statistics in uniform field will therefore converge towards the following averages [26, 27] :

- energy loss,

$$\Delta E = \frac{2}{3} r_0 E_0 \gamma^4 \frac{\Delta s}{\rho^2} = \frac{2}{3} r_0 e c \gamma^3 B \frac{\Delta s}{\rho} \tag{3}$$

(an other form of the familiar relation $\Delta E/E \approx 1.88\ 10^{-15}\ \gamma^3 \Delta\theta/\rho$),

- energy spread

$$\sigma_{\Delta E/E} = \frac{\sqrt{110\sqrt{3}\hbar c\ /\ \pi\epsilon_0}}{24E_0/e}\ \gamma^{5/2}\ \frac{\sqrt{\Delta\theta}}{\rho} \tag{4}$$

(which writes $\sigma_{\Delta E/E} = 3.80\ 10^{-14}\ \gamma^{5/2}\sqrt{\Delta\theta}/\rho$, for electrons).

Note that, unless otherwise specified, notations in this study assume $\beta = v/c \approx 1$.

2.2.3 Benchmarking, preliminary steps

At this stage, the installation of the Monte Carlo machinery in Zgoubi can be benchmarked for these quantities, assuming, following the hypotheses in appendix A, iso-magnetic lattice and $\rho = 24.95549$ m. From a practical point of view, in order to stick to ideal theoretical conditions, a single bend is tracked once-through, so to avoid such effects as orbit spiraling, momentum spread, that may be sensible over a large ring or in presence of RF compensation.

Results are given in Tab. 1. The classical, theoretical formulæ used are recalled in the rightmost column, synchrotron radiation integrals invoked here and elsewhere in the text ($I_n, n = 1, 5$) are recalled in appendix B. E_s is the total energy of the reference particle, $\mathcal{C}_\gamma = \frac{4\pi}{3}\frac{r_0}{(m_0c^2)^3}$. The values so computed are for 6 GeV kinetic energy, they are converged numerically, up to the last digit shown in the table, in terms of the integration step size in the bend (about 1 cm step size) and of the number of radiated photons (made large enough, via the number of passes), this is discussed in appendix C.

It can be seen that the agreement between Zgoubi tracking data (col. 3 in Tab. 1) and theoretical expectations (col. 4) is very good, this is a first step towards validation the SR Monte Carlo installation in Zgoubi. Monte Carlo losses at higher energies also yield good agreement with theory, this will be addressed further in section 4.

Table 1: Preliminary benchmarking : SR loss characteristics in the Chasman-Green cell described in appendix A. These quantities have been computed from a large number of once-through passes, of a 3000 particle batch, in a single dipole, they are shown here scaled to a full turn (64 such dipoles). Kinetic energy considered is 6 GeV.

	Units	Zgoubi tracking	Theory value	formula (SI units)
Energy loss, U_s	MeV / turn	4.59565	4.59565	$\frac{\mathcal{C}_\gamma}{2\pi} E_s^4 I_2 \overset{iso-\rho}{=} \mathcal{C}_\gamma \frac{E_s^4}{\rho}$
Critical photon energy, ϵ_c	keV	19.2049	19.2051	$\frac{3\hbar\gamma^3 c}{2\rho}$
Average photon energy, $\bar{\epsilon}$	keV	5.9136	5.9136	$\frac{8}{15\sqrt{3}}\epsilon_c$
Nb. of average photons	/turn/particle	777.12	777.12	$U_s/\bar{\epsilon}$
rms energy spread, $\sqrt{(\epsilon-\bar{\epsilon})^2}$	keV	10.7375	10.7375	$\frac{\sqrt{211}}{15\sqrt{3}}\epsilon_c$

2.2.4 Scattering

SR effects on particle dynamics are either limited to the change of particle energy, or may include scattering, namely, a change in the direction of the momentum vector due to the angle of emission of the photon with respect to that vector, in which case a third random process, namely the photon emission angle, may be accounted for.

Trajectory scattering may assume for simplicity a cylindrical-symmetric Gaussian distribution

$$p(\xi) = \exp(-\frac{\xi^2}{2\sigma_\xi^2}) \tag{5}$$

of the photon emission angle ξ with respect to the particle velocity. For simplicity as well σ_ξ may be considered independent of photon energy ϵ, with value $\approx 1/\gamma$. Whether these two approximations hold may be problem dependent, however these hypotheses may easily be improved in the code if this is found necessary.

Accounting for scattering is an option in Zgoubi. Since its effect on beam divergence is very small in the present benchmarking conditions (mainly a matter of asymptotic vertical invariant value), it does not need be (and is not) taken into account.

2.2.5 Field scaling

Particle stiffness decrease upon SR loss entails increased strength of the magnets, in particular the curvature in dipoles, $1/\rho$. In the case of single-pass beam lines, this effect may be taken care of so as to keep the bending and focusing strength of the optical elements unchanged, by scaling of the magnetic fields to the *theoretical* average energy loss, namely (Eq. 3)

$$\Delta E_{scaling} = \sum_{bends} \frac{2}{3} r_0 e c \gamma^3 B \Delta\theta \tag{6}$$

Note the following : (i) using that analytical expression in computing the scaling coefficient is preferred to the average energy loss from the tracked particle population, since in the latter case it would make it dependent on the accuracy of the statistics ; (ii) on the other hand, in the present state of Zgoubi coding, that scaling is only accounted for in dipole type of magnetic fields. However the code provides analytical models of a number of magnets, including multipoles of arbitrary order, FFAG style magnets, etc. [1, 2], and accounting for that scaling factor can be extended to those if necessary (a matter of short Fortran developments in the routines of concern, more on that can be found in the Users' Guide [2]).

When simulating storage rings, bends and lenses are normally operated at fixed field, thus the RF takes care of restoring on average the energy lost, given appropriate synchronous RF phase in the cavity device(s) in Zgoubi. In pulsed regime as in booster injectors, the same process of energy recovery on average by the RF can be simulated as well.

3 Benchmarking method

Benchmarking of the Monte Carlo SR in Zgoubi is based on the monitoring of the only data that the code can produce : particle coordinates, versus time or turn number. Other quantities, such as motion excursions, invariants, concentration ellipses (see appendix D), emittance ratios, etc., are derived from these coordinates.

A storage ring is considered in the present simulations, the ring includes an RF cavity for compensation of the SR induced energy loss. The cavity is located at the end of the structure, its properties are detailed in appendix A.2. A sample of typical Zgoubi tracking data and of their manipulation can be found in appendix E. Various quantities out of Zgoubi are investigated in the present study, they are made explicit in section 3, the goal of the benchmarking is to have their values compared with expectations from the Chasman-Green cell theory.

This study will be limited obviously, to some of the main aspects of the effects of synchrotron radiation on beam dynamics. However Zgoubi data files corresponding to the results produced in the following, in both coupled and uncoupled optics cases, have been stored in the "exemple" folder in the Zgoubi SourceForge development site [2, 3], from where they may be downloaded in view of further investigations.

Motion invariants

In the absence of perturbation by synchrotron radiation, particle motion satisfies the following invariants,

$$\epsilon_z = \gamma_z(s) z^2 + 2\alpha_z(s) z z' + \beta_z(s) z'^2 \quad \text{Courant-Snyder} \tag{7}$$

$$\epsilon_l = \frac{\alpha E_s}{2\Omega_s} \left[\left(\frac{\Delta E}{E_s} \right)^2 + \frac{1}{\Omega_s^2} \left(\frac{d}{dt} \frac{\Delta E}{E_s} \right)^2 \right] \quad \text{longitudinal} \tag{8}$$

$$(\widehat{\Delta E})^2 = (\Delta E)^2 + \frac{1}{\Omega_s^2} \left(\frac{d\Delta E}{dt} \right)^2 \quad \text{amplitude squared} \tag{9}$$

with z = x or y the horizontal or vertical transverse coordinate, β_z and $\alpha_z = -\beta_z'/2$ the Twiss parameters, $\Delta E = E - E_s$ the energy offset, E_s the reference energy, $\Omega_s = (\omega_{\rm rev}^2 |\eta| h_{\rm RF} e\hat{V} \cos\phi_s \,/\, 2\pi E_s)^{1/2}$ the synchrotron angular frequency, with $\eta = 1/\gamma^2 - \alpha \approx -\alpha$ the phase slip factor, α the momentum compaction. $h_{\rm RF}$ is the RF harmonic, $\omega_{\rm rev} = 2\pi/T_{\rm rev}$ the revolution angular frequency, $\hat{V}$ the

RF peak voltage, ϕ_s the synchronous phase (numerical values considered for these latter quantities in the benchmarking exercises are given in appendix A).

Introducing the squared rms relative synchrotron amplitude $\sigma^2_{\widehat{\frac{\Delta E}{E}}} \equiv (\widehat{\Delta E}/E_s)^2$, Eqs. 8 and 9 lead to the following relationship

$$\epsilon_l = \frac{\alpha E_s}{2\,\Omega_s}\,\sigma^2_{\widehat{\frac{\Delta E}{E}}} \tag{10}$$

Note that in the present simulations, particle motion is observed in a non-dispersive region in the cell (namely, at the azimuth $s = 0$ (Fig. 9 in appendix A), thus there is no need to subtract the effect of the dispersion function on the horizontal phase space coordinates, when evaluating the emittances from the tracking. Note in addition that, in the following, unless otherwise specified, emittances are taken rms, unnormalized.

Under the effect of stochastic SR, individual invariants can in general not be determined, averages over particle ensembles are considered instead, they evolve according to

$$\frac{d\overline{\epsilon}_n}{dt} = -\frac{\overline{\epsilon}_n}{\tau_n} + C_n \tag{11}$$

($\overline{(*)}$ denotes the average over particles ; $\epsilon_n = \epsilon_x,\ \epsilon_y$ or ϵ_l ; at fixed energy (storage ring) C_n is a constant, characteristic of the quantum excitation, which will be made explicit in due place) towards a stationary solution

$$\epsilon_{n,eq} = C_n\,\tau_n \tag{12}$$

with damping time

$$\tau_n = \frac{T_{rev}\,E_s}{U_s\,J_n} \tag{13}$$

with $J_{n=x,y,l}$ the partition numbers, respectively horizontal, vertical, longitudinal, which, in passing, satisfy (the Robinson theorem)

$$J_x + J_y + J_l = 4 \tag{14}$$

Note that the present benchmarking simulations consider for simplicity a planar ring (parameters defined in appendix A), with the effect that the vertical motion is not subject to chromatic orbit fluctuations, by contrast with the horizontal betatron motion which experiences orbit fluctuations upon stochastic energy loss. It is thus possible to compute the vertical invariant and follow its smooth evolution turn by turn, from a single particle tracking. This will be addressed specifically in the next section.

4 Beam dynamics simulations

Based on the working hypotheses and methods discussed in section 3, a series of multi-turn tracking simulations has been performed for the benchmarking of Zgoubi synchrotron radiation Monte Carlo machinery. In order for the simulation conditions to be closer to the Chasman-Green lattice theory synchrotron radiation is only allowed in the bends (no SR in quadrupoles and sextupoles).

The simulations involve bunches of 2000 to 6000 particles depending on the exercise, tracked over several damping times. Several runs, however in rather limited number, have been performed in each case, with various initial conditions, random generator seeds, this will not be detailed here. Due to the limited number of trials, error bars can be up to a few percent level, depending on the parameters of concern, which is anyway considered indicative of the correct behavior of Zgoubi in matter of SR simulation and its effects.

In addition to Zgoubi tracking and to theoretical formulæ, the light source code BETA [28] developed at Saclay was used in this benchmarking, as a follow on of the above mentioned initial benchmarking work in beamlines [4]. Determination of SR parameters in BETA is based on the computation of the radiation integrals, from the lattice parameters. Some results are given in appendix F.

Uncoupled motion is investigated first, the results are summarized in the next three sections, in the form essentially of figures and tables.

4.1 Damping of the vertical motion

The vertical motion is considered first, using single particle tracking following the planar ring hypotheses as discussed in section 3. A 18 GeV particle is launched for 500 turns (10 damping times about) in the 16-cell ring. Since there is no vertical dispersion, its vertical phase space coordinates y, y' are expected to show no stochastic fluctuation, this is confirmed by the smoothly spiraling phase space motions observed in Fig. 1. From these coordinates the vertical invariant can be computed, namely,

$$\epsilon_y = \gamma_y y^2 + 2\alpha_y y y' + \beta_y y'^2 \tag{15}$$

with local values of β_y, α_y as given in appendix A. The invariant ϵ_y is expected to damp exponentially towards zero, with a theoretical damping time (Eq. 13 with $J_y = 1$)

$$\tau_y = \frac{T_{rev}\,E_s}{U_s} \approx 0.13114 \text{ ms, or } \frac{E_s}{U_s} \approx 48.06 \text{ turns} \tag{16}$$

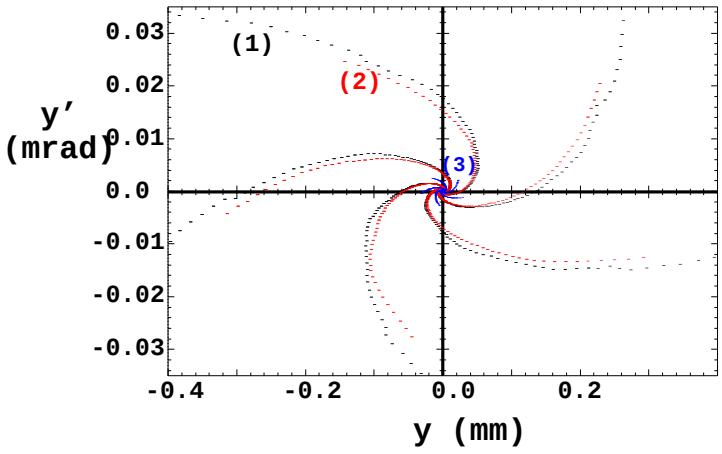

Figure 1: Vertical phase space of four particles with different starting invariants, 18 GeV (as detailed in Fig. 2 - motion of particle 4 is too small to be visible here). Motions are observed over 500 turns at $s = 0$ ($s = 0$ is defined in Fig. 9, appendix A).

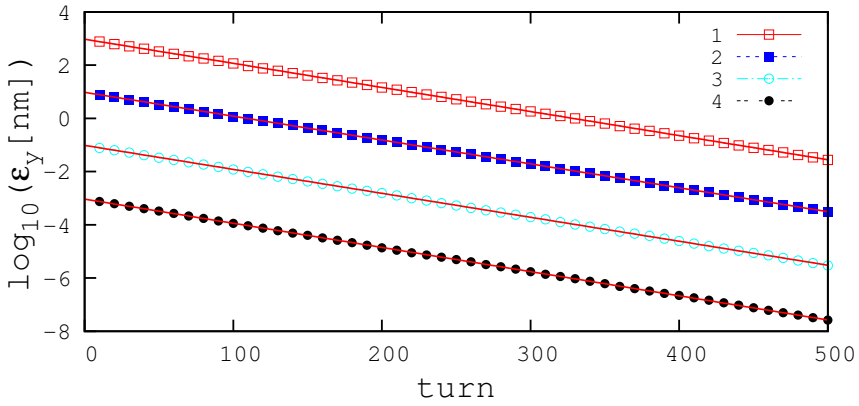

Figure 2: Exponential damping of the single-particle vertical invariant ϵ_y, over 500 turns, 18 GeV (markers, from Zgoubi tracking, matched using Eq. 15). Case of four particles with starting invariants differing by six orders of magnitude, respectively, from 1 to 4 : $10^3,\ 10,\ 10^{-1}$ and 10^{-3} nm. Corresponding damping times from a linear fit (solid lines) fall within 130.33 ± 0.2 (ms).

given $E_s = 18$ GeV, theoretical energy loss $U_s = 372.16$ MeV/turn (from formula in Tab. 1) and $T_{rev} = 2.711216\ \mu$s. This is confirmed in Fig. 2 which shows smooth exponential damping of the vertical invariant on the one hand, in four different cases of starting initial invariant values spanning eight orders of magnitude, yielding on the other hand damping time in accord with Eq. 16 at better than 1.5 per mill accuracy, for all four starting invariant values.

Additional simulation results concerning the vertical motion will be produced in the next section.

4.2 Emittance evolution

Multi-particle tracking is now investigated in either one of the three planes, horizontal, vertical or longitudinal. The tracking is carried out up to equilibrium, $\epsilon_{n,eq}$, i.e., a few damping times away. Four different energies are considered : 6, 9, 12 and 18 GeV, kinetic.

For all three motions, transverse and longitudinal, the evolution of the emittance with time or turn number, t, is expected to satisfy

$$\bar{\epsilon}_n(t) = \epsilon_{n,eq}\left(1 - e^{-t/\tau_n}\right) + \epsilon_{n,i}\, e^{-t/\tau_n} \quad (n = x,\ y,\ \text{or}\ l) \tag{17}$$

with $\epsilon_{n,i}$ and $\epsilon_{n,eq}$ respectively the starting and equilibrium emittances.

A case of longitudinal emittance growth is illustrated in Fig. 3, starting with initial beam emittance $\epsilon_{l,i} = 0$. Horizontal emittance damping is illustrated in Fig. 4, with initial emittance $\epsilon_{x,i} > \epsilon_{x,eq}$. Some aspects of these Zgoubi tracking outcomes, their manipulation and unit conversions are discussed in appendix E. These figures show the good matching between the emittances computed from the tracking coordinates (5000 particles for each energy), and Eq. 17. Note that Fig. 4 is obtained with a single cavity in the ring, whereas with one cavity per cell instead (16 cavities total), the asymptotic value $\epsilon_{x,eq}$ comes out slightly less, closer to $\frac{\mathcal{C}_q\gamma^2}{J_x\rho}\bar{\mathcal{H}}$ (see Tab. 2).

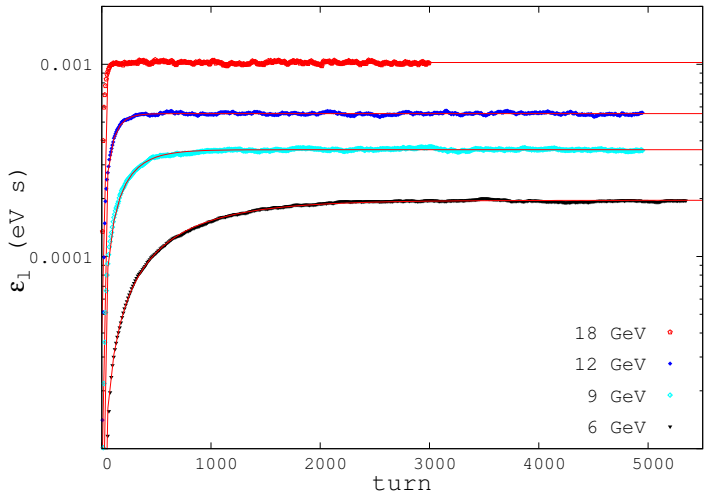

Figure 3: Evolution of the longitudinal emittance with turn number, starting with $\epsilon_{l,i} = 0$, in four different cases of energy, 6, 9, 12 and 18 GeV. Markers are from tracking (not all turns are shown. 5000 particles tracked per energy), solid lines are from matching with the exponential law (Eq. 17).

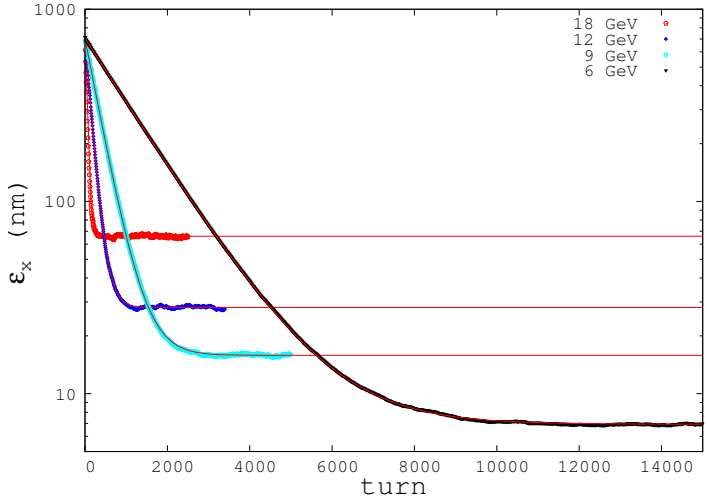

Figure 4: Damping of the horizontal emittance with turn number toward $\epsilon_{x,eq}$, in four different cases of energy, 6, 9, 12 and 18 GeV. Markers are from tracking (not all turns are shown), solid lines are from matching with the exponential law (Eq. 17). This results are obtained in the case of a single energy loss compensation cavity in the ring.

The matching yielded the damping times τ_l, τ_x and the equilibrium emittances $\epsilon_{l,eq}$, $\epsilon_{x,eq}$, as reported in Tab. 2. Agreement between Zgoubi tracking in the presence of stochastic SR on the one hand, and theoretical expectations on the other hand, is within 1-3 percent.

On the other hand, since these simulations consider a planar ring, the vertical emittance damps to zero, $\epsilon_{y,eq}(t \to \infty) \to 0$, so yielding

$$\bar{\epsilon}_y(t) = \epsilon_{y,i}\, e^{-t/\tau_y} \quad \text{and} \quad \ln(\bar{\epsilon}_y(t)) = \ln(\epsilon_{y,i}) - \frac{t}{\tau_y} \tag{18}$$

This produces the results displayed in Fig. 5 which shows the smooth damping, as due to the absence of fluctuations in the vertical motion in the absence of vertical dispersion, for a 2000 particle bunch tracked for 10 damping times about, in the four different cases 6, 9, 12 and 18 GeV. A linear regression on the logarithmic set of turn-by-turn emittances $\bar{\epsilon}_y(t)$ yields the matching straight line as displayed, for each energy, of which the absolute value of the inverse slope is the damping time, values as reported in Tab. 2, rightmost column. The agreement with theory is good, at percent level. The phase space angle

$$\phi_y = \text{atan}\frac{\alpha_y y + \beta_y y'}{y} \tag{19}$$

is also computed, it is expected to feature a uniform density distribution in the $[-\pi, \pi]$ interval, which Fig. 6 shows to be fairly satisfied.

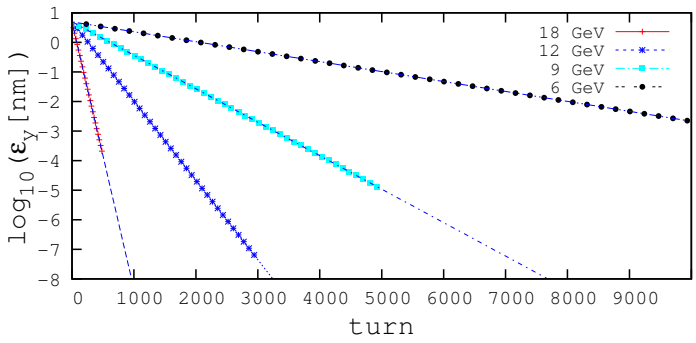

Figure 5: Smooth damping of the vertical emittance towards zero, for 6, 9, 12 and 18 GeV, 2000 particles tracked. Markers are from the tracking (not all turns are shown), straight lines are from the exponential match (Eq. 18).

Table 2: Dependence of the energy loss, damping times, and longitudinal and horizontal equilibrium emittances, on the kinetic energy, as obtained from Zgoubi tracking over 10 damping times and more. A 2000 particle bunch has been tracked for τ_y, 5000 for all other quantities. Values between square brackets are the theoretical expectations (formulæ of concern are gathered in the bottom row, for convenience). Note the presence of two tracking outcomes in the "$\epsilon_{x,eq}$" column : the upper value is obtained in the case of a single RF cavity in the ring, the lower one is in the case of an RF cavity at each cell (a total of 16 around the ring).

	Energy loss U_s (MeV/turn)	$\epsilon_{l,eq}$ (μeV.s)	σ_l (mm)	τ_l (ms)	$\epsilon_{x,eq}$ (nm)	τ_x (ms)	τ_y (ms)
Scaling :	γ^4	$\gamma^{3/2}$	$1/\gamma^{1/2}$	$1/\gamma^3$	γ^2	$1/\gamma^3$	$1/\gamma^3$
6 GeV	4.5956 *[4.5956]*	196 *[192]*	9.37 *[9.309]*	1.769 *[1.769]*	6.90 *[6.83]*	3.547 *[3.546]*	3.501 *[3.540]*
9 GeV	23.263 *[23.263]*	358 *[352]*	7.67 *[7.601]*	0.548 *[0.524]*	$\frac{15.87}{15.60}$ *[15.37]*	1.020 *[1.051]*	1.040 *[1.049]*
12 GeV	73.518 *[73.518]*	554 *[542]*	6.67 *[6.582]*	0.225 *[0.221]*	$\frac{28.18}{28.04}$ *[27.32]*	0.447 *[0.443]*	0.439 *[0.443]*
18 GeV	372.16 *[372.16]*	1022 *[996]*	5.42 *[5.375]*	0.068 *[0.066]*	$\frac{65.77}{63.24}$ *[61.46]*	0.132 *[0.131]*	0.130 *[0.131]*
Theory	$\frac{\mathcal{C}_\gamma}{2\pi} E_s^4 I_2 = \mathcal{C}_\gamma \frac{E_s^4}{\rho}$	$\frac{\alpha E_s}{2\Omega_s}\sigma^2_{\widehat{\frac{\Delta E}{E}}} = \frac{\alpha E_s}{\Omega_s}\frac{\mathcal{C}_q\gamma^2}{J_l\,\rho}$	$\frac{\alpha c}{\Omega_s}\sigma_{\frac{\Delta E}{E}}$	$\frac{3T_{rev}}{2r_0\gamma^3(2I_2+I_4)} = \frac{T_{rev}E_s}{U_s J_l}$	$\frac{\mathcal{C}_q\gamma^2}{J_x}\frac{I_5}{I_2} = \frac{\mathcal{C}_q\gamma^2}{J_x\rho}\bar{\mathcal{H}}$	$\frac{3T_{rev}}{2r_0\gamma^3(I_2-I_4)} = \frac{T_{rev}E_s}{U_s J_x}$	$\frac{3T_{rev}}{2r_0\gamma^3 I_2} = \frac{T_{rev}E_s}{U_s J_y}$

Uniform distributions as well, not worked out here, are expected for the horizontal phase space angle ϕ_x, as well as for the longitudinal angle

$$\phi_l = \text{atan}\frac{d\Delta E/dt}{\Omega_s \Delta E} \tag{20}$$

Other possible benchmarking tests would concern the beam centroids, expected to damp to zero with damping times $2\tau_n$, this has been checked to be satisfied, on various cases, not reported here. The equilibrium distribution of any of the phase space variables, x, x', ΔE, etc. is also a test of the correctness of the SR process simulation, they have to match Gaussian densities, with rms width for instance

$$\sigma_x(s) = \left(\beta_x(s)\frac{\mathcal{C}_q\gamma^2}{J_x\rho}\bar{\mathcal{H}} + D_x^2(s)\sigma^2_{\frac{\Delta E}{E}}\right)^{1/2},$$
$$\sigma_{\frac{\Delta E}{E}} = \frac{1}{\sqrt{2}}\sigma_{\widehat{\frac{\Delta E}{E}}} = \sqrt{\frac{\mathcal{C}_q}{J_l\rho}}\gamma \tag{21}$$

with $D_x(s)$ the local dispersion, $\mathcal{C}_q = \frac{55}{32\sqrt{3}}\frac{\hbar}{m_0 c} \approx 3.832\times10^{-13}$ m. Various of these rms values have been benchmarked, they are reported in Tab. 2.

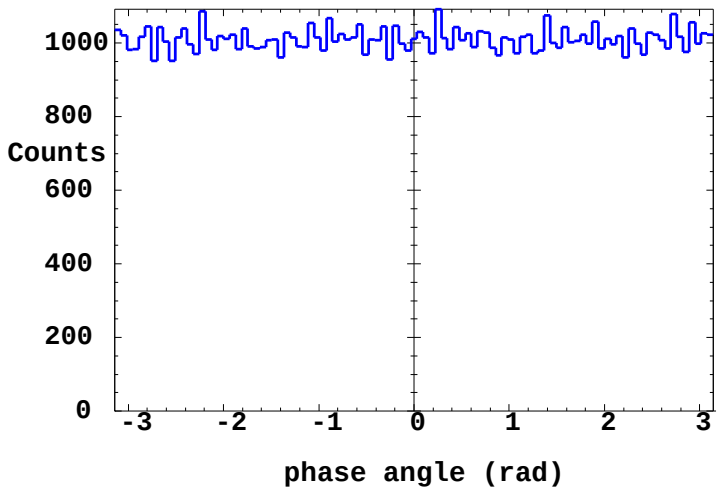

Figure 6: Histogram of the phase space angle (Eq. 19) over 10^5 particle phase space positions after a few damping time tracking, beam energy 12 GeV.

A note on damping without fluctuations : The horizontal and longitudinal damping times might be obtained with high accuracy by tracking a single particle and by accounting for the energy loss *on average, without fluctuations*, instead. A matching of the turn-by-turn evolution of the invariant (respectively, Eq. 7 with $z = x$ and Eq. 8) would then provide the damping time as the absolute value of the inverse slope of the straight line representing $\ln(\overline{\epsilon}_n(turn))$ ($n = x$ or l), given that $\epsilon_{n,eq} = 0$ in the absence of stochasticity. However it is a deliberate choice here to benchmark the code in realistic situation, in the presence of stochastic photon emission using the Monte Carlo machinery installed for that. The counterpart is that it requires a two-variable matching : damping time and final emittance. It is left to the interested user, as a further benchmarking test, to replace (in the code) the random energy loss by the average energy loss, and then verify the exponential damping of a single particle invariant, in that special configuration of the Zgoubi machinery.

4.3 Energy dependence

Benchmarking for energy dependence of equilibrium emittances and damping times is summarized in Tab. 2. Damping times are obtained by matching the turn-by-turn emittance with equations 17 or 18, as in Figs. 3, 4, 5. Emittances are obtained by matching the turn-by-turn emittance with equation 17, as in Figs. 3, 4.

Expected γ-scaling laws are recalled (3rd row in the table), as well as energy loss (2nd column). Values between square brackets are the expected theoretical ones (from the formulæ in the bottom "Theory" row). A limited number of tracking trials have been realized in general for any of these quantities, their average value is displayed in the table. In spite of this limited statistics, the agreement is rather satisfactory, within a few percent or better, better in particular for the vertical motion which is not subject to stochasticity. Differences with formulæ may have various origins, *e.g.*, oscillations due to mis-centering of the beam at injection, fluctuations with turn number due to the limited number of particles, cumulative effects due to the single recovery cavity (spiraling for instance), non-linear effects from the sextupoles, whereas the theoretical formulæ invoked for comparison (bottom two rows in Tab. 2) assume a perfectly iso-magnetic configuration, this remains to be investigated further, a work in progress.

5 Coupled motion

5.1 Working hypotheses

The source of induced vertical emittance in this coupling simulation is a single skew quadrupole (short enough that the geometry of the lattice can be considered unchanged) introduced in a dispersion free drift (s=0, Fig. 9). The difference resonance $Q_x - Q_y = 25$ is considered, the lattice is tuned to $Q_x \approx 36.2$, $Q_y \approx 11.2$, see Fig. 10. $Q_x - Q_y - 25 = \Delta$ is the distance of the unperturbed tunes difference to an integer, with Δ small.

A perturbative treatment of coupling in the presence of synchrotron radiation can be found in Ref. [29]. A coupling strength is defined,

$$\kappa = \frac{1}{4\pi} \oint K_s \sqrt{\beta_x \beta_y} e^{i(\psi_x - \psi_y - \Delta 2\pi s/\mathcal{C})}\, ds \tag{22}$$

with $K_s = \frac{1}{2\,B\rho}\left(\frac{\partial B_x}{\partial x} - \frac{\partial B_y}{\partial y}\right)$ the skew quadrupole strength, $\beta_{x,y}$ (respectively $\psi_{x,y}$) the local uncoupled horizontal and vertical betatron functions (phase advances) at the skew quadrupole, $\mathcal{C}$ the ring circumference. Note that the notation $|C^-| = 2|\kappa|$ is sometimes used instead, entailing different forms for equations 24, 25 [29]. In the presence of a single skew quadrupole Eq. 22 yields the approximation

$$|\kappa| \approx \frac{|K_s L|}{4\pi} \sqrt{\beta_x \beta_y} \tag{23}$$

with $K_s L$ the integrated skew quadrupole strength.

The equilibrium beam emittances are expected to evolve following (the earlier "*eq*" (equilibrium) subscript has been dropped in the following, for simplicity)

$$\epsilon_x = \epsilon_{x,0} \frac{2|\kappa|^2 + \Delta^2}{4|\kappa|^2 + \Delta^2}, \quad \epsilon_y = \epsilon_{x,0} \frac{2|\kappa|^2}{4|\kappa|^2 + \Delta^2} \tag{24}$$

and their ratio is expected to satisfy

$$\frac{\epsilon_y}{\epsilon_x} = \frac{|\kappa|^2}{|\kappa|^2 + \Delta^2/2} \tag{25}$$

The sum of the transverse emittances is expected to be invariant, equal to the natural horizontal emittance,

$$\epsilon_x + \epsilon_y = \epsilon_{x,0} \tag{26}$$

5.2 Typical tracking simulation

A first numerical experiment is performed at 6 GeV. The thin-lens skew quadrupole has an integrated gradient of 0.06 T. The working

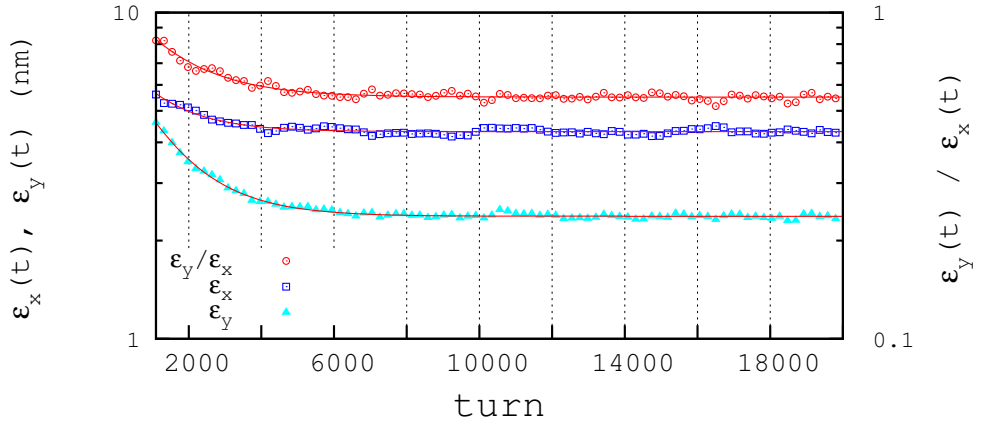

Figure 7: Evolution of horizontal and vertical emittances with turn (not all turns are shown), in presence of coupling (left vertical axis), and their ratio (right axis). Markers are from Zgoubi tracking. An exponential fit (solid curves) yields the asymptotic values in Tab. 3, bottom row.

conditions are summarized in Tab. 3. A 5000 particle bunch is tracked for 20000 turns, *i.e.*, 15 transverse emittance damping times about. Eq. 31 still holds in deriving emittances from the particle coordinates, since the coupling does not change the horizontal dispersion, and in particular both the skew quadrupole and the observation point are in a non-dispersive straight. The results of the tracking are displayed

Table 3: Coupling simulations at 6 GeV. The left two columns give the unperturbed tunes, the third one gives the distance to an integer. The rightmost four columns give respectively the expected uncoupled natural emittance $\epsilon_{x,0}$ (from the formula in Tab. 2), the expected equilibrium emittances (Eq. 24) and their ratio (Eq. 25). The equilibrium emittances and their ratio from an exponential fit of the tracking data (as displayed in Fig. 7) are given in the bottom row, rightmost four columns, for comparison.

Q_x	Q_y	$\Delta = \lvert Q_x - Q_y - 25\rvert$	$\lvert K_s L\rvert$ (m^{-1})	β_x (m)	β_y (m)	$\lvert\kappa\rvert$	Equilibrium emittances $\epsilon_{x,0}$	ϵ_x (nm)	ϵ_y	Ratio ϵ_y/ϵ_x
36.203	11.198	$5\,10^{-3}$	$3\,10^{-3}$	26.6	11.3	$4.2\,10^{-3}$	6.83	4.34	2.49	0.575
							6.83	4.31	2.38	0.557

in Fig. 7. Matching of the exponential decay towards the horizontal and vertical emittances yields the three numerical values for the equilibrium emittances in the bottom row in Tab. 3, differing respectively by less than 1%, 5% and 4% from the expected values, rightmost three columns in Tab. 3.

5.3 Emittance ratio and sum

This second exercise is performed at higher energy, 18 GeV (for the sake of computing speed). 5000 particle bunches are tracked for 800 turns, *i.e.*, 16 emittance damping times about. The tracking is iterated for several values of the coupling strength $|\kappa|$ (by changing the skew quadrupole strength $K_s L$), with fixed distance Δ from the tune diagonal. The working conditions are, paraxial, unperturbed : $Q_x = 36.175$, $Q_y = 11.18$, $\beta_x = 26.5$, $\beta_y = 11.4$. Compared to the previous exercise, the tunes have been moved to a region free of non-linear coupling resonance (see appendix A.3 and Fig. 10).

A summary of the tracking results regarding equations 25, 26 is given in Fig. 8. Tracking data (markers in the figure) are superimposed with these analytical expectations. Up to a strong $|\kappa|/\Delta \approx 5$, $(\epsilon_x + \epsilon_y)$ falls within $\pm 5\%$ of $\epsilon_{x,0} \approx 65\,\mathrm{nm}$. Beyond that limit, $(\epsilon_x + \epsilon_y)/\epsilon_{x,0}$ increases, the reason for that would require further investigation, however, as opposed to the perturbative hypothesis above, strong coupling changes the optical functions and tunes [29, 30], the latter are moved away from one another (that effect might be quantified from a Fourier analysis of Zgoubi tracking data).

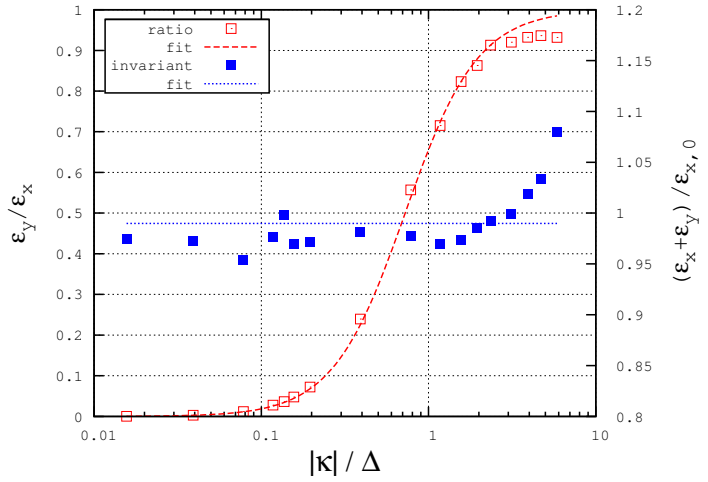

Figure 8: Left vertical scale : evolution of the ratio of vertical to horizontal equilibrium emittances with coupling strength, from Zgoubi tracking (empty red markers), and their interpolation using equation 25 (red "fit" curve). Right scale : $(\epsilon_x + \epsilon_y)/\epsilon_{x,0}$ ratio at equilibrium as a function of coupling strength, from tracking (solid blue markers) and their average value (horizontal dashed blue line).

6 Comments, conclusions

Stepwise ray-tracing of 6-D motion in Zgoubi in presence of synchrotron radiation has been investigated based on a Chasman-Green lattice, including conditions of coupled optics. Numerical values have been put on a number of quantities such as energy loss, damping times, equilibrium emittances, emittance ratio. They appear to yield good agreement with the analytical theory of the Chasman-Green

cell, so bringing confidence in the correctness of the Monte Carlo SR machinery installation on the one hand, and on the accuracy of the numerical tracking in presence of SR and its stochastic effects on beam dynamics, on the other hand. All the exercises discussed here can be repeated using the input data files stored in the Zgoubi SourceForge development site [3].

Beyond these elementary aspects, the benchmarking of the code could of course be pushed further with a more complicated structure, *e.g.*, including Robinson wigglers, by further comparison with appropriate tracking codes for instance.

A conclusion that can be drawn from the present investigations is that no unexpected result was obtained, neither any show stopper faced, all the simulations undertaken have given expected data with reasonable accuracy. CPU times are reasonable, 1000 turns per minute for one particle, in the 812 meter ring - for an arbitrary number of particles on a CPU cluster.

The computational material for the investigation of SR induced spin diffusion combines spin tracking capabilities in Zgoubi, together with beam dynamics effects of SR as addressed here. It is thus operational, benchmarking against theory will essentially be a matter of adding spin dynamics to the tracking simulations in the presence of stochastic energy loss. In such ring as eRHIC energy recovery recirculator in the electron-ion collider project, the reduced number of turns (of the order of 10) and the CPU speed achieved will allow statistical estimates on electron beam polarization and perturbative effects based on tens of thousands of particles [11].

APPENDIX

A Chasman-Green test lattice

A.1 Properties

A Chasman-Green cell (*aka* double-bend achromat, DBA) is considered in the present benchmarking study, for the reason that a number of quantities relevant to beam dynamics under SR effects can be derived analytically in that case, as the chromatic invariant $\mathcal{H}$, equilibrium emittances, damping times, etc. The formulæ of concern in the benchmarking have been gathered in Tabs. 1, 2, 6, they are drawn from Refs. [26, 27] or other classical textbooks.

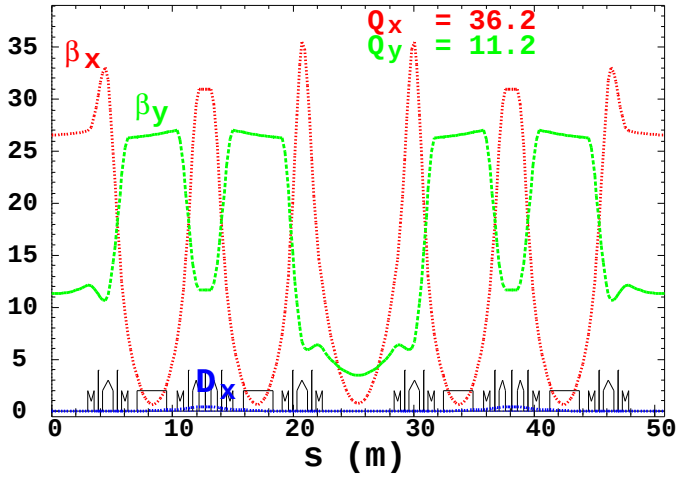

Figure 9: Optical functions (in meters, left vertical scale) along the Chasman-Green cell.

Table 4: Ring parameters, as set in the tracking simulations, and other numerical data used in the main text as obtained from Zgoubi tracking. Corrected chromaticities are accounted for in the present benchmarking simulations.

1	Cell length	(m)	50.800
2	Number of cells		16
3	Circumference, $\mathcal{C} = 2\pi R$	(m)	812.800
4	momentum compaction, α	(10^{-4})	3.098
5	Qx		36.20
6	Qy		11.20
7	Q'x, Q'y, natural		-114, -34.5
8	Q'x, Q'y, corrected		+0.035, -0.012
	Bend parameters :		
9	Nb. of bends		64
10	Bend deviation, θ	(rad)	$2\pi/64$
11	Bend length, $\mathcal{L}$	(m)	2.45
12	Curvature radius, ρ	(m)	24.95549
	Periodic functions at non-dispersive dipole end :		
13	β_0	(m)	3.415
14	α_0		2.073
	Periodic functions at s=0 :		
15	β_x, β_y	(m)	26.6088, 11.3027
16	α_x, α_y		0

A variant of the early times[3] ESRF super-cell is used, including chromaticity sextupoles. A storage ring is built from 16 such super-cells, whereas various storage energies will be considered, taken in the range 6 GeV (actual ESRF energy) to 18 GeV.

Tab. 4 gives the general optical parameters of the lattice and ring, the optical functions are displayed in Fig. 9.

[3]The ESRF lattice has been modified in the recent past.

A.2 RF conditions

SR losses in bends over the ring circumference amount to

$$U_s = \frac{\mathcal{C}_\gamma}{2\pi}\,\beta^3\,E_s^4\,I_2 \approx \frac{\mathcal{C}_\gamma}{2\pi}\,E_s^4\,I_2 \overset{iso-\rho}{=} \mathcal{C}_\gamma\frac{E_s^4}{\rho}$$

or, ultra-relativistic electrons,

$$U_s[keV/turn] \approx 88.463\frac{E_s^4[GeV]}{\rho[m]}$$

yielding for instance

$$U_s \approx 4.6 \text{ MeV/turn at 6 GeV,} \quad 2.45 \text{ MW power}$$

Numerical values, for 6 GeV electrons, are given in Tab. 1. The radiated energy is restored by the RF system. A single cavity is accounted for in the present simulations, with parameters as listed in Tab. 5.

Table 5: RF conditions in Zgoubi simulations, longitudinal parameters.

Revolution time, T_{rev}	$(10^{-6}s)$	2.71122
Frequency, $f_{rf} = \omega_{rf}/2\pi$	(MHz)	110.651
Harmonic, $h_{\rm RF}$		300
Synchronous phase, φ_s	(deg)	30
Peak voltage, $\hat{V}$	(MV)	$9.19123\times\left(\frac{E_s[GeV]}{6.000511}\right)^4$
Synchrotron tune, Q_s		$0.004430\times\left(\frac{E_s[GeV]}{6.000511}\right)^{3/2}$

A.3 Coupled optics

The precise positioning of the working point is not a concern in the non-coupled numerical experiments, first part of the note, since there is no source of non-linear coupling excitation, apart from kinematic terms present by nature in the Zgoubi method, however negligible given the paraxial working conditions. That working point happens to be located at (A), Fig. 10.

By contrast, in the case of the coupled optics the working point is located in a resonance line free diamond, point (B) in Fig. 10. This is in order to fulfill the coupling formalism hypothesis of an isolated linear coupling resonance. Chromaticities are below 0.1 so ensuring small footprint well within the resonance-free diamond.

Note that it has been observed that, performing similar coupling simulations with working point (A) instead, straddling sum coupling resonance lines, jeopardizes the invariance of $\epsilon_x + \epsilon_y$ when $\kappa/\Delta \gtrsim 0.5$, to be compared to similar effect for $\kappa/\Delta \gtrsim 5$ instead, with working point (B),

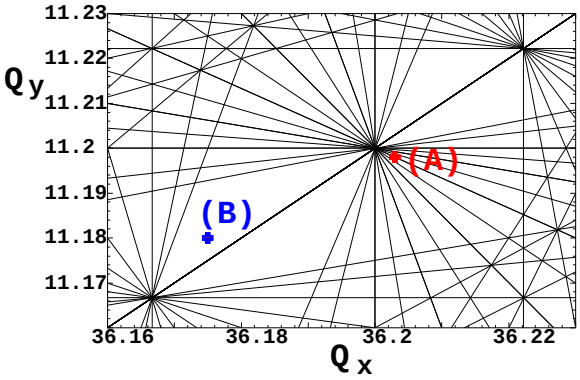

Figure 10: Working points. (A) uncoupled case. (B) coupled case, away from coupling resonance lines $mQ_x + nQ_y = p$, p integer, represented up to order $|m| + |n| = 10$ here.

B Synchrotron radiation integrals

Tab. 6 recalls the expressions for the SR integrals [26, 27], as used in the paper.

Table 6: SR integrals and their expression in the case of the Chasman-Green cell, iso-magnetic lattice.

($\oint \equiv$ integral over the dipoles)		Units
$I_1 = \oint \frac{D_x}{\rho(s)}\, ds$	$= \alpha\mathcal{C}$	(m)
$I_2 = \oint \frac{ds}{\rho(s)^2}$	$= \frac{2\pi}{\rho}$	(m^{-1})
$I_3 = \oint \frac{ds}{\lvert\rho(s)\rvert^3}$	$= \frac{2\pi}{\lvert\rho\rvert^2}$	($10^{-2}\mathrm{m}^{-2}$)
$I_4 = \oint \frac{D_x}{\lvert\rho(s)\rvert^3}(1-2n)\, ds$	$= \frac{1}{\lvert\rho\rvert^3}\oint D_x ds$ $^{(a)}$	($10^{-4}\mathrm{m}^{-1}$)
$I_5 = \oint \frac{\mathcal{H}}{\lvert\rho(s)\rvert^3}\, ds$	$= \frac{2\pi}{\lvert\rho\rvert^2}\bar{\mathcal{H}}$ $^{(b)}$	($10^{-5}\mathrm{m}^{-1}$)
$\bar{\mathcal{H}} = \frac{1}{2\pi\rho}\oint_{bends} \mathcal{H} ds$	$\overset{(CG)}{=} \rho\theta^3(\frac{\gamma_0\mathcal{L}}{20} + \frac{\beta_0}{3\mathcal{L}} - \frac{\alpha_0}{4})$ $^{(b)}$	(mm)

(a) $n = -\rho/B\ \partial B/\partial x$ field index, zero here, ρ is the curvature radius in bends.
(b) $\mathcal{H} = \gamma_x D_x^2 + 2\alpha_x D_x D'_x + \beta_x D'^2_x$. "$(CG)$" : case of Chasman-Green lattice. D_x is the dispersion, D'_x its derivative, α, β, γ are the optical functions, the subscript "0" denotes their values at entrance to the first bend in the cell (Fig. 9).

C Numerical convergence

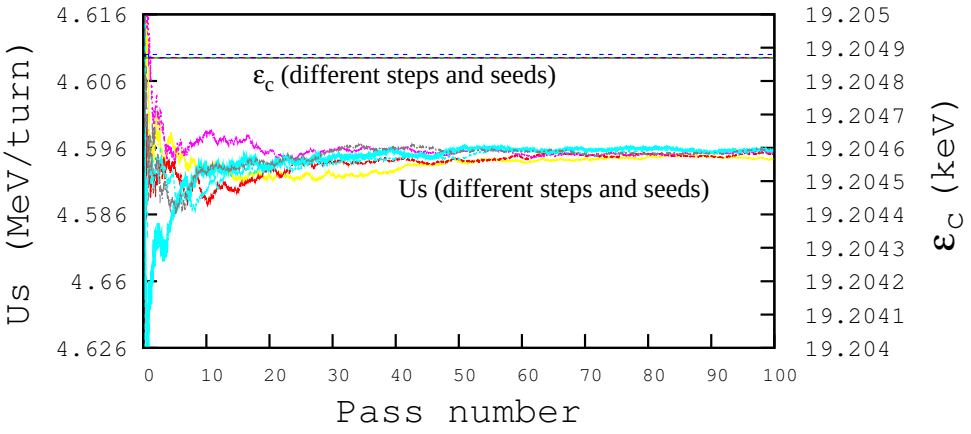

Figure 11: Convergence (running average) of the energy loss U_s towards 4.5956 MeV/turn (lower curve bundle, left vertical scale), and of the critical frequency ϵ_c towards 19.205 keV (top curve bundle, right vertical scale), as a function the number of passes of a 3000 particle batch, through the 2.45 m cell dipole, at 6 GeV. The various curves in each one of these two bundles (essentially superimposed in the ϵ_c case) correspond to different Monte Carlo seeds and different integration step sizes in the dipole).

In order to perform a preliminary convergence test on the Monte Carlo SR loss installation in Zgoubi, a 3000 particle batch is launched for a large number of passes through a single dipole of the Chasman Green cell. The dipole is 2.45 m long (Tab. 4), the test is performed at 6 GeV kinetic energy. Fig. 11 displays the results of several trials, involving three different sets of random generator seeds (for the Monte Carlo SR simulations), various integration step sizes in the bend (5 mm to 10 cm). It shows that the average energy loss U_s gets close to its asymptotic value in a few tens of once-through passes across the dipole. The average of the critical energy ϵ_c is reached even faster.

D Concentration ellipses

Several comparisons discussed in this report lean on the concentration ellipses, which are a standard product out of Zgoubi data treatment tools, such as its interactive interface zpop [2]. In order to make things clear, we recall briefly the way they are computed in the code,

from the coordinates of the particles.

Let $z_i(s),\ z_i'(s)$ be the phase space coordinates of $i = 1, n$ particles observed at some azimuth s, at some turn around the ring. The second moments of the particle distribution are

$$\begin{aligned} \overline{z^2}(s) &= \frac{1}{n}\sum_{i=1}^{n}(z_i(s) - \overline{z}(s))^2 \\ \overline{zz'}(s) &= \frac{1}{n}\sum_{i=1}^{n}(z_i(s) - \overline{z}(s))(z_i'(s) - \overline{z'}(s)) \\ \overline{z'^2}(s) &= \frac{1}{n}\sum_{i=1}^{n}(z_i'(s) - \overline{z'}(s))^2 \end{aligned} \tag{27}$$

From these, a concentration ellipse (CE) is drawn, of surface $\mathcal{S}_z(s)$ and equation

$$\gamma_c(s)z^2 + 2\alpha_c(s)zz' + \beta_c(s)z'^2 = \mathcal{S}_z(s)/\pi \tag{28}$$

Noting $\Delta = \overline{z^2}(s)\,\overline{z'^2}(s) - \overline{zz'}^2(s)$, the ellipse parameters write

$$\begin{aligned} \gamma_c(s) = \overline{z'^2}(s)/\sqrt{\Delta},\ \ \alpha_c(s) = -\overline{zz'}(s)/\sqrt{\Delta}, \\ \beta_c(s) = \overline{z^2}(s)/\sqrt{\Delta},\ \ \mathcal{S}_z(s) = 4\pi\sqrt{\Delta} \end{aligned} \tag{29}$$

With these conventions, the rms values of z and z' projections satisfy

$$\sigma_z = \sqrt{\beta_z \mathcal{S}_z/\pi} \quad \text{and} \quad \sigma_{z'} = \sqrt{\gamma_z \mathcal{S}_z/\pi} \tag{30}$$

In addition, in the first order formalism, given that the observation point in these simulations is taken in a non-dispersive region ($s = 0$ in Fig. 9), one has, by comparison with Eq. 7,

$$\mathcal{S}_z(s)/\pi \equiv \epsilon_z \tag{31}$$

E Sample Zgoubi tracking outcomes

Typical data out of Zgoubi tracking and their manipulation are discussed here. The energy considered is 6 GeV, 2000 particles were tracked and yielded the horizontal and longitudinal equilibrium emittances and other bunch length values in Tab. 2.

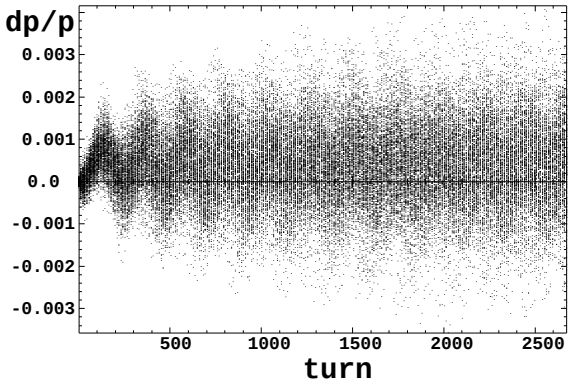

Figure 12: Energy spread build-up with turn toward its equilibrium value, at 6 GeV.

Figure 12 shows a plot of the momentum spread dp/p which is one of the particle coordinates in Zgoubi. Starting from zero emittance, the momentum spread builds up with turns, toward the theoretical equilibrium rms value $\sigma_{\frac{\Delta E}{E}} = \sqrt{\frac{\mathcal{C}_q}{\mathcal{J}_l \rho}}\gamma$. The RF frequency happens to have a slight offset, so causing the visible beam centroid oscillation, which damps toward its equilibrium value (a few 10^{-4}) in a time twice the emittance damping tine.

Figure 13 shows the longitudinal phase space portrait, taken at 5 damping times about (region of turn number 3000) where it has grown close to its asymptotic shape. Together with dp/p, the RF phase ϕ is part of the particle data saved during Zgoubi tracking. Other

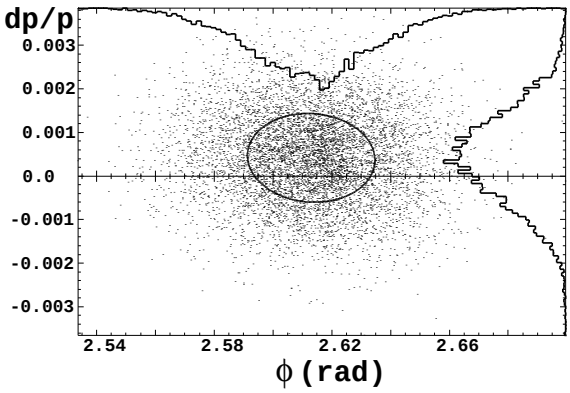

Figure 13: Longitudinal phase space portrait at 6 GeV, turn number 3000, in Zgoubi tracking coordinates RF phase ϕ and dp/p. The surface of the rms ellipse for the 2000 particles, in these coordinates, is $22\,10^{-6}\,\pi$ rad.

quantities as emittance in various possible units, bunch length, etc., are derived from these. The projected coordinate densities in the figure, respectively RF phase ϕ (horizontal axis) and dp/p (vertical axis) yield the following rms values,

$$\sigma_{\frac{\Delta E}{E}} = 1.02\,10^{-3}, \quad \sigma_{\Delta\phi} = 21.3\,\text{mrad}$$

The phase extent can be converted to bunch length, as follows,

$$\sigma_l = \frac{c\sigma_{\Delta\phi}}{2\pi f_{rf}} = 9.2\,\text{mm}$$

with c the speed of light and given the RF frequency value $f_{rf} = 110.7\,\text{MHz}$ (Tab. 5). Given a factor of $1/2\pi f_{rf} = 1.44\,10^{-9}$ for the phase, and of $p = \beta E \approx E = 6\,10^9$ eV for the energy, the phase-dp/p emittance $\epsilon_l = 22\,10^{-6}$ rad so converts into $190\,10^{-6}$ eV.s.

F Comparisons with BETA

The light source code BETA [28] has been used to assess various of the parameters discussed in this report, for comparison with Zgoubi's Monte Carlo. Outcomes are satisfactory, as can be seen in Tab. 7.

Damping times in the "Zgoubi" column in the table are obtained by matching the turn-by-turn emittance with equations 17 or 18, emittances are obtained by matching the turn-by-turn emittance with equation 17.

Table 7: Comparisons with BETA. Data in the "Theory value" column are from the formulæ in the rightmost column. The definition of the synchrotron integrals, $I_1 - I_5$ and $\bar{\mathcal{H}}$ as used here is recalled in appendix B.

	Units	BETA code	Zgoubi	Theory value	formula
horizontal, τ_x	ms turns	3.546 1308	3.547 1308	3.547 1308	$= \frac{T_{rev} E_s}{U_s J_x} = \frac{3 T_{rev}}{2 r_0 \gamma^3 (I_2 - I_4)}$
vertical, τ_y	ms turns	3.540 1306	3.501 1291	3.541 1306	$= \frac{T_{rev} E_s}{U_s J_y} = \frac{3 T_{rev}}{2 r_0 \gamma^3 I_2}$
longitudinal, τ_l	ms turns	1.769 652	1.757 648	1.769 652	$= \frac{T_{rev} E_s}{U_s J_l} = \frac{3 T_{rev}}{2 r_0 \gamma^3 (2 I_2 + I_4)}$
horizontal, $\epsilon_{x,eq}$	nm	6.843	6.83	6.831	$= \frac{\mathcal{C}_q \gamma^2}{J_x} \frac{I_5}{I_2} \overset{iso-\rho}{=} \frac{\mathcal{C}_q \gamma^2}{J_x \rho} \bar{\mathcal{H}}$
vertical, $\epsilon_{y,eq}$	pm	-	$\rightarrow 0$	$\approx$0.15	$= \frac{13}{55} \frac{C_q}{J_y I_2} \oint \frac{\beta_y}{\lvert\rho^3\rvert} ds$
longitudinal, $\epsilon_{l,eq}$	μeV.s	192.1	193.5	191.8	$= \frac{\alpha E_s}{2 \Omega_s} \sigma^2_{\widehat{\frac{\Delta E}{E}}} = \frac{\alpha E_s}{\Omega_s} \frac{\mathcal{C}_q \gamma^2}{J_l \rho}$
$rms\ dE/E$, $\sigma_{\frac{\Delta E}{E}} = \frac{1}{\sqrt{2}} \sigma_{\widehat{\frac{\Delta E}{E}}}$	10^{-3}	1.03	1.023	1.028	$= \sqrt{\frac{\mathcal{C}_q}{J_l \rho}} \gamma$
rms bunch length, σ_l	mm	9.31	9.40	9.308	$= \frac{\alpha c}{\Omega_s} \sigma_{\frac{\Delta E}{E}}$

References

[1] F. Méot, *The ray-tracing code Zgoubi - status*, NIM A 767 (2014) 112-125.

[2] The "Zgoubi Users' Guide" can be found at
http://www.scienceaccelerator.gov/dsa/result-list/fullRecord:zgoubi/
Source files as well as many examples (input and output data files, ranging from beam lines to spectrometers to high energy colliders) are available at the SourceForge development site http://sourceForge.net/projects/zgoubi/. Zgoubi's data treatment/analysis interface program, zpop, as well as a toolkit with many additional treatment/analysis tools, can be found at the latter address as well.

[3] Copies of the data files for the present study have been saved in the SourceForge development site, at http://sourceForge.net/p/zgoubi/code/HEAD/tree/trunk/, in the folder "SRDampingInESRFRing" : the uncoupled optics cases are in the sub-folders "6GeV", "9GeV", "12GeV", "18GeV", a coupled optics data file (the Sec. 5.2 case) is in the sub-folder "coupled".

[4] F. Méot, J. Payet, *Numerical tools for the simulation of synchrotron radiation loss and induced dynamical effects in high energy transport lines*, internal report DAPNIA/SEA-00-01, CEA/DSM Saclay (July 2000).

[5] P. Lapostolle, F. Méot, S. Valero, *A new dynamics code DYNAC for electrons, protons and heavy ions in LINACS with long accelerating elements*, 1990 LINAC Conf., Albuquerque, NM, USA ; report SATURNE/GT/90-04, CEA/DSM Saclay (1990).

[6] *Electron Laboratory For Europe, "Blue Book"*, Accelerator Technical Proposal, CNRS-IN2P3 editor, Institut des Sciences Nucléaires, Grenoble, France (1994).

[7] G. Leleux, P. Nghiem, A. Tkatchenko, *Synchrotron radiation perturbation in transport lines*, IEEE 1991 Particle Accelerator Conference, San Francisco, USA, May 6-9, 1991.

[8] V. Ptitsyn et al., *High luminosity electron-hadron collider eRHIC*, http://accelconf.web.cern.ch/AccelConf/IPAC2011/papers/thpz019.pdf.

[9] F. Méot, *A numerical method for combined spin tracking and ray tracing of charged particles*, NIM A 313 (1992) 492-500.

[10] F. Méot et al., *Lattice design and study tools regarding the super-B project*, Procs. IPAC10, Kyoto, Japan, 2010.

[11] F. Méot, *End-to-end 9-D polarized bunch transport in FFAG eRHIC*, EIC14 workshop, http://www.jlab.org/conferences/eic2014/.

[12] M. Borland, *elegant : A Flexible SDDS-Compliant Code for Accelerator Simulation*, Tech. Note LS-287, Advanced Photon Source, September 2000. The user manual is on line at <http://www.aps.anl.gov/Accelerator_Systems_Division /Accelerator_Operations_Physics/oagSoftware.shtml>. Synchrotron radiation is simulated in one of two ways : 1/ As a lumped element, using the SREFFECTS element. 2/ Element-by-element, using CSBEND, KQUAD, and KSEXT elements, M. Borland, ANL, private communication, March 2014.

[13] SAD (Strategic Accelerator Design) home page, KEK : <http://www.lepp.cornell.edu/~dcs/bmad/manual.html>. "SAD can track particles with synchrotron radiation. [...] each magnet is split into several slices. Inside the slice, a particle obeys symplectic map and at each border of slices it loses momenta/energy randomly depending on the magnetic field felt by the particle.".

[14] The Bmad manual can be obtained at <http://www.lepp.cornell.edu/ dcs/bmad/manual.html> ; the manual does not cover the bend radiation algorithm ; essentially, the algorithm involves a spline interpolation to the standard radiation integrals ; the bend radiation code is in the file bmad/photon/photon_init_mod.f90, D.C. Sagan, Cornell, private communication, March 2014.

[15] MAD documentation is available at http://hansg.web.cern.ch/hansg/mad/mad8/doc/.

[16] S. Redaelli et al., *Comparison of different tracking codes for beam delivery systems of linear colliders*, Proceedings of EPAC 2002, Paris, France.

[17] F. Méot, A. Verdier, *Effect of the undulator in IR4 on the LHC beam*, CERN LHC Project Note 343 (2004).

[18] L. Ponce, F. Méot, *Undulator radiation simulation tools in view of proton beam diagnostics in LHC*, SL-Note-2001-038/BI, CERN, 25 Sept. 2001.

[19] Y. Dutheil et al., Polarization profile and spin dynamics simulations in the AGS using the Zgoubi code; Y. Dutheil et al., Spin dynamics simulations and horizontal intrinsics resonance studies in the AGS using Zgoubi, Proceedings of NA-PAC 2013 Conference, Pasadena, CA.

[20] F. Méot et al., *Polarization transmission at RHIC, numerical simulations*, Proceedings of IPAC2012, New Orleans, Louisiana, USA.
F. Méot et al., Spin code benchmarking at RHIC, Proceedings of 2011 Particle Accelerator Conference, New York, NY, USA.

[21] F. Méot et al., *Spin tracking simulations in AGS based on ray-tracing methods*, internal report C-AD/AP/452, Sept. 2009.

[22] This research used resources of the National Energy Research Scientific Computing Center, which is supported by the Office of Science of the U.S. Department of Energy under Contract no. DE-AC02-05CH11231.

[23] S.C. Tygier, Modeling Space Charge in an FFAG with Zgoubi, Proceedings of IPAC2012, New Orleans, Louisiana, USA.

[24] C. Bovet, A. Burns, F. Méot, M. Placidi, E. Rossa, J. De Vries, *Synchrotron radiation interferences between short dipoles at LEP*, rep. CERN SL/97-59 (BI), Nov. 1997. http://www.osti.gov/scitech/biblio/562080.
F. Méot, *A theory of low frequency, far-field synchrotron radiation*, Particle Accelerators, Vol. 62 (1999), pp. 215-239.

[25] L. Ponce, R. Jung, F. Méot, *LHC proton beam diagnostics using synchrotron radiation*, Yellow Report CERN-2004-007.

[26] A. Hofmann, *The Physics of Synchrotron Radiation*, Cambridge University Press (2004).

[27] M. Sands, *The Physics of Electron Storage Rings: An Introduction*, SLAC Report 121 (1970). Available at http://www.slac.stanford.edu/pubs/slacreports/slac-r-121.html

[28] L. Farvacque et al, *BETA users' guide*, ESRF, third edition (2001).
https://oraweb.cern.ch/pls/hhh/code_website.disp_code?code_name=BETA

[29] G. Guignard, *Betatron coupling and related impact of radiation*, Phys. Rev. E 51 61046118 (1995).

[30] Y. Luo, *Transverse beam sizes and quasi emittances for linear coupled optics*, NIM A 562 (2006) 57-64.